UNIVERSITY OF TRENTO
DEPARTMENT OF PHYSICS
BACHELOR'S DEGREE IN PHYSICS

~ · ~

ACADEMIC YEAR 2023–2024

BUBBLES IN A FERROMAGNETIC SUPERFLUID

Supervisor
Dr. Alessandro ZENESINI

Graduate Student
Giorgio MICAGLIO
227051

FINAL EXAMINATION DATE: March 10, 2025

To all my friends

Acknowledgments

I would like to thank all of my friends.

Abstract

This thesis analyses an experiment observing bubbles in a ferromagnetic superfluid formed through false vacuum decay. The aim of this work is to characterize the bubbles in order to retrieve their most important properties and relating them to the parameters of the experiment.

Contents

Introduction **1**

1 Theoretical background **3**
1.1 Ideal Bose gas . . . 3
1.2 Gross-Pitaevskii equation . . . 5
1.3 Two-component spin mixture . . . 6
1.4 Coherently coupled mixture . . . 7
1.5 False vacuum decay and bubble formation . . . 7

2 Data analysis **9**
2.1 Experimental platform . . . 9
2.2 Data . . . 9
2.2.1 Bubble parameters and shot sorting . . . 10
2.2.2 FFT and ACF analysis . . . 11
2.2.3 Border alignment . . . 12

Conclusions **15**

Bibliography **17**

List of Figures **19**

Introduction

This thesis originates from the first experimental observation of False Vacuum Decay (FVD), made by the Pitaevskii BEC Center laboratories of the University of Trento and presented in Ref. [3].

Chapter 1

Theoretical background

In this chapter we will briefly discuss the theoretical background used when dealing with two-component coherently coupled spin mixtures of BECs. Since we are dealing with a many-body quantum problem, the standard approach is to use a quantum field to describe the state of the condensate. This leads directly to the Gross-Pitaevskii equation, which will be the starting point of this discussion, after a quick review of the ideal Bose gas. The following content is mostly based on Refs. [2] and [1].

1.1 Ideal Bose gas

The simplest way to treat the ideal Bose gas (a quantum system of non-interacting bosons) is by relying on the grand-canonical ensemble.

Let us then recall the probability of the system having a number of particles N' and energy E_k when in contact with a reservoir of temperature T and chemical potential μ:

$$P_{N'}(E_k) = e^{\beta(\mu N' - E_k)}\,,$$

with $\beta = 1/(k_B T)$, from which one can build the *grand-canonical partition function*

$$\mathcal{Z}(\beta,\mu) = \sum_{N'=0}^{\infty}\sum_{k} P_{N'}(E_k) = \sum_{N'=0}^{\infty} e^{\beta\mu N'} Q_{N'}(\beta)\,, \tag{1.1}$$

where $Q_{N'}$ is the canonical partition function associated to a system of N' (fixed) particles. From the partition function, the physical properties of the system are derived through the calculation of the grand-canonical potential

$$\Omega = E - TS - \mu N = -k_B T \log \mathcal{Z}\,. \tag{1.2}$$

In the case of a non-interacting system, the total Hamiltonian is $H = \sum_i H_i$, where the single-particle Hamiltonian solves the eigenvalue problem $H_i\phi_i(\mathbf{r}) = \epsilon_i\phi_i(\mathbf{r})$. In this setting, each energy level ϵ_i is occupied by n_i particles, and thus the total number of particles and the total energy are

$$N' = \sum_i n_i\,, \qquad E_k = \sum_i \epsilon_i n_i\,.$$

The partition function of Eq. (1.1) becomes easy to compute, yielding

$$\mathcal{Z}(\beta,\mu) = \sum_{n_0=0}^{\infty}\sum_{n_1=0}^{\infty}\cdots\; e^{\beta\mu\sum_i n_i} e^{-\beta\sum_i \epsilon_i n_i} = \left(\sum_{n_0} e^{\beta\mu n_0} e^{-\beta\epsilon_0 n_0}\right)\left(\sum_{n_1} e^{\beta\mu n_1} e^{-\beta\epsilon_1 n_1}\right) =$$
$$= \prod_i \sum_{n_i}\left[e^{\beta(\mu-\epsilon_i)}\right]^{n_i} = \prod_i \frac{1}{1-e^{\beta(\mu-\epsilon_i)}}\,.$$

Note that the condition $\mu < \epsilon_0$ must be satisfied for the convergence of the series. It is interesting to study the total number of particles, which can be obtained from the potential of Eq. (1.2):

$$N = \langle N'\rangle = -\frac{\partial\Omega}{\partial\mu} = k_B T\frac{\partial \log\mathcal{Z}}{\partial\mu} = \sum_i \frac{1}{e^{\beta(\epsilon_i-\mu)}-1} = \sum_i \langle n_i\rangle\,,$$

hence revealing the famous *Bose-Einstein distribution*

$$\langle n_i\rangle = \frac{1}{e^{\beta(\epsilon_i-\mu)}-1}\,.$$

The occupation number of the ground state is $N_0 = \langle n_0\rangle$ and the remaining particles are called the thermal component $N_T = N - N_0$.

The origin of the Bose-Einstein condensation phenomenon is that $N_0 \to \infty$ when $\mu \to \epsilon_0$. In particular, at a fixed temperature T, the function $N_T(\mu)$ has a maximum N_c at $\mu = \epsilon_0$, while N_0 is divergent. This implies that:

- if $N_c > N$, then the normalization condition $N = N_0 + N_T$ is satisfied for values of $\mu < \epsilon_0$ and N_0 is negligible (no condensation);
- if $N_c = N$, it means that we are at the critical temperature T_c defined by $N_T(T = T_c, \mu = \epsilon_0) = N$. Since N_T is an increasing function of T, the previous scenario corresponds to $T > T_c$;
- if $N_c < N$ (or $T < T_c$), the contribution of N_0 is crucial for the normalization and thus the condensation happens.

In a finite box of volume V, where the lowest energy eigenvalue is $\epsilon_0 = 0$, the condensate fraction for $T < T_c$ is expressed by

$$\frac{N_0}{N} = 1 - \left(\frac{T}{T_c}\right)^{3/2}\,.$$

Since $N_0 \approx 0$ for $T > T_c$, the function has a discontinuity of its derivative at the critical temperature: a typical symptom of phase transitions.

The behaviour is similar for a system trapped in an external harmonic potential, where the condensate fraction is

$$\frac{N_0}{N} = 1 - \left(\frac{T}{T_c}\right)^3$$

and the critical temperature depends on the oscillation frequencies.

1.2 Gross-Pitaevskii equation

For a 1D single-component BEC, namely made of only one species of N indistinguishable bosons, one can use a single wavefunction $\psi(x,t)$ to describe its ground state (GS) by exploiting a mean-field approximation, thus revealing the Gross-Pitaevskii equation (GPE):

$$i\hbar\frac{\partial\psi(x,t)}{\partial t} = \left[-\frac{\hbar^2}{2m}\nabla^2 + V(x,t) + g|\psi(x,t)|^2\right]\psi(x,t)\,. \tag{1.3}$$

The unusual term in this equation is the one proportional to the square modulus of the wavefunction through the constant g, called the *contact interaction constant*, that describes the interactions between bosons. In fact, for an ideal gas of non-interacting bosons, $g = 0$ and one retrieves the standard Schrödinger equation, but this situation is not realistic for our purposes. The interaction constant can be written in terms of the boson-boson scattering length a, a typical property of elastic collisions, by

$$g = \frac{4\pi\hbar^2}{m}a\,,$$

with $g > 0$ for a stable BEC (for $g < 0$ the system is unstable and collapses on itself).

The GPE can be written in its stationary form as

$$\left[-\frac{\hbar^2}{2m}\nabla^2 + V(x) + g|\psi(x)|^2\right]\psi(x) = \mu\psi(x)\,, \tag{1.4}$$

where $\mu \approx \frac{\partial E}{\partial N}$ is the chemical potential and accounts for the energy contribution of a single particle. Spatial properties of the condensate can arise from this equation, especially in the case of $N \gg 1$ and when the interaction term is dominating. By neglecting the kinetic energy term from Eq. (1.4), one easily gets the stationary solution

$$|\psi(x)|^2 = n(x) = \frac{\mu - V(x)}{g}\,,$$

where $n(x)$ is the density distribution, and the association of the latter with the square modulus of the wavefunction leads to the normalization condition $\int|\psi(x)|^2\mathrm{d}x = N$. A relevant case is when the external potential is harmonic, yielding a parabolic distribution

$$n(x) = \frac{\mu - \frac{1}{2}m\omega^2x^2}{g} = 0 \qquad \Leftrightarrow \qquad x = R_{\mathrm{TF}} = \sqrt{\frac{2\mu}{m\omega^2}}\,,$$

with R_{TF} being the Thomas-Fermi radius, a parameter indicating the spatial confinement of the condensate.

Another important property to study is the elementary excitations spectrum due to small perturbations of the GS. It is called the Bogoljubov spectrum and yields

$$E(k) = \hbar\omega(k) = \sqrt{\frac{\hbar^2k^2}{2m}\left(\frac{\hbar^2k^2}{2m} + 2mc^2\right)} \approx \begin{cases}\hbar ck & \text{if} \quad \hbar k \ll mc \\ \frac{\hbar^2k^2}{2m} & \text{if} \quad \hbar k \gg mc\end{cases}\,.$$

Also, the healing length is a quantity that expresses how small can spatial changes of the wavefunction be at most. It is

$$\xi = \frac{1}{\sqrt{8\pi na}} = \frac{\hbar}{\sqrt{2mng}}\,.$$

1.3 Two-component spin mixture

When the system is composed of two different species (a and b), Eq. (1.4) splits into two coupled stationary GPEs:

$$\left[-\frac{\hbar^2}{2m}\nabla^2 + V(x) + g_{aa}|\psi_a(x)|^2 + g_{ab}|\psi_b(x)|^2\right]\psi_a(x) = \mu_a\psi_a(x)\,,$$
$$\left[-\frac{\hbar^2}{2m}\nabla^2 + V(x) + g_{ab}|\psi_a(x)|^2 + g_{bb}|\psi_b(x)|^2\right]\psi_b(x) = \mu_b\psi_b(x)\,.$$

This is due to the possibility of collisions not only between bosons a-a or b-b, but also of the type a-b, thus producing three interaction constants g_{aa}, g_{bb}, g_{ab}. Depending on those constants' values, the system can assume different behaviours and GS configurations.

For example, take the case of a flat box potential in a total fixed volume V, yielding constant densities. Letting $n_a = |\psi_a|^2$ and $n_b = |\psi_b|^2$, we can express the energy density in the following way:

$$\mathcal{E} = \frac{1}{2}g_a n_a^2 + \frac{1}{2}g_b n_b^2 + g_{ab}n_a n_b - \mu_a n_a - \mu_b n_b\,,$$

where the first three terms represent the interactions between particles of the same type and between different ones, while the last two terms account for the chemical potentials. Now, we state that the system is thermodynamically stable and miscible if and only if the Hessian of $\mathcal{E}$ with respect to n_a and n_b is positive-definite. The calculation is straight-forward:

$$H = \begin{bmatrix} \frac{\partial^2\mathcal{E}}{\partial n_a^2} & \frac{\partial^2\mathcal{E}}{\partial n_a \partial n_b} \\ \frac{\partial^2\mathcal{E}}{\partial n_a \partial n_b} & \frac{\partial^2\mathcal{E}}{\partial n_b^2} \end{bmatrix} = \begin{bmatrix} g_a & g_{ab} \\ g_{ab} & g_b \end{bmatrix} > 0 \qquad \Leftrightarrow \qquad \begin{cases} g_a > 0 \\ g_b > 0 \\ g_a g_b > g_{ab}^2 \end{cases}.$$

The first two conditions ensure that neither a nor b collapse, while the latter expresses the condition for miscibility. Intuitively, if g_{ab} is small with respect to the other constants, it means that the two species do not interact much one with the other, thus letting themselves mix and spatially overlap. On the other hand, if g_{ab} is big (and positive), they strongly repulse and undergo a phase separation. From now on, only repulsive interactions will be considered, so the only possibilities will be immiscible or miscible (no collapse).

In the more general case of a non-uniform trapping potential, the densities depend from the position and the distributions are correlated with the interaction constants. Considering the harmonic trap and the miscible case, if $g_a > g_b$ then the species b will be confined in a small central region, while the species a will occupy more space. This is shown in the lower section of Fig. 1.1, while the upper section shows the immiscible case and the buoyancy (again, $g_a > g_b$). One notes that the total density profile is not Thomas-Fermi anymore when $g_a \neq g_b$.

It is natural to wonder what the excitation spectrum might look like when two components are present, especially when there is spatial overlap between them. The Bogoljubov spectrum of Eq. (1.2) is preserved, but now divided into two energy channels, namely spin and density:

$$E_{d,s}(k) = \hbar\omega_{d,s}(k) = \sqrt{\frac{\hbar^2k^2}{2m}\left(\frac{\hbar^2k^2}{2m} + 2mc_{d,s}^2\right)}\,,$$

with the speeds of sound ($+$ for the density and $-$ for the spin) being

$$c_{d,s}^2 = \frac{(g_a n_a + g_b n_b) \pm \sqrt{(g_a n_a - g_b n_b)^2 + 4g_{ab}^2 n_a n_b}}{2m}\,.$$

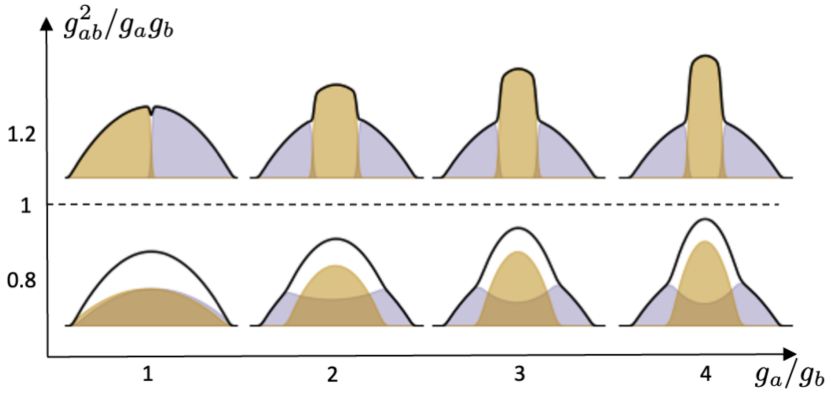

Figure 1.1: GPE simulation of a two-component balanced mixture in a harmonic potential. The shaded purple region shows the density distribution of population a and the yellow one the population b. Here, a small magnetic field is used to break the left-right simmetry. The total density profile is drawn in black.

There are also two distinct healing lengths,

$$\xi_{d,s} = \frac{\hbar}{\sqrt{2}mc_{d,s}}\,.$$

1.4 Coherently coupled mixture

When the system is composed of two species of the same atom, such as two hyperfine states, the dynamics become more interesting because of the possible interconversion processes. One possibility is to use a homogeneous microwave radiation, which couples the two internal states $|a\rangle$ and $|b\rangle$, of the type

$$\Omega_R(t)\exp\Big\{-i\omega_{\text{cpl}}t+\phi\Big\}\,,\qquad \omega_{\text{cpl}}=\omega_{ab}+\delta\,,$$

where the coupling frequency ω_{cpl} differs from the transition frequency between the state ω_{ab} by a parameter δ called *detuning*.

1.5 False vacuum decay and bubble formation

Given the asymmetric double well describing the mean-field energy landscape of the condensate (Fig. 1.2), the metastable state A in which all atoms are in the state $|\uparrow\rangle$ is called False Vacuum (FV), since it is not the true ground state. The possibility of tunneling to the state B arises from the fact that the bubble formation has an energy cost due to the kinetic contribution of the interaction on the interface (domain wall) between atoms $|\uparrow\rangle$ and $|\downarrow\rangle$. However, when a sufficient number of atoms in the core region flips to $|\downarrow\rangle$, the energy gain compensates the kinetic cost and the tunneling can occur resonantly from A to B. Once happened, the system is

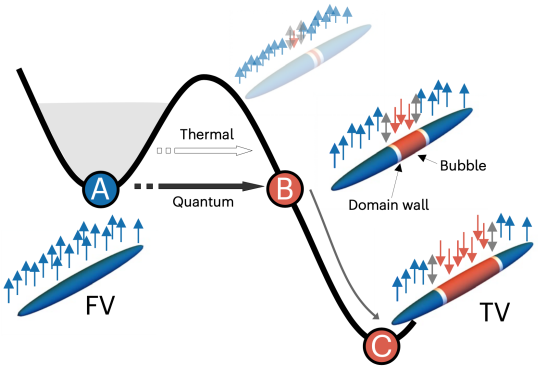

Figure 1.2: Mean field energy and bubble formation.

not in a metastable state anymore, hence the decaying into C, the True Vacuum (TV), via bubble expansion.[1]

What is interesting to study is the energy dissipation of the decay during the expansion. The key point is that since the coherent coupling prohibits the system to emit photons, the energy must dissipate through the spin and/or density channel, possibly with waves. Investigating this phenomenon is the purpose of this thesis' data analysis.

[1]Note that the TV is not composed of all atoms $|\downarrow\rangle$. This is because while the $|\downarrow\rangle$ state is energetically lower in the high-density core region, the situation is opposite in the low-density tails.

Chapter 2

Data analysis

In this chapter we will talk about the experimental platform in which the experiment was carried out and we will then proceed with the FFT and ACF data analysis.

2.1 Experimental platform

The experimental platform is composed of a bosonic gas of ^{23}Na atoms, optically trapped and cooled below the condensation temperature. The initial spin state in which the system is prepared is $|F, m_F\rangle = |2, -2\rangle = |\uparrow\rangle$, with F being the total angular momentum of the atom ($\mathbf{F} = \mathbf{I} + \mathbf{J}$, takes into account the nuclear spin and the total angular momentum of the electrons) and m_F its projection on the quantization axis. The $|\uparrow\rangle$ state is then coupled to $|1, -1\rangle = |\downarrow\rangle$ through microwave radiation with amplitude Ω_R. The relevant scattering lengths concerning the two states are $a_\uparrow = 64.3a_0$, $a_\downarrow = 54.5a_0$ and $a_{\uparrow\downarrow} = 64.3a_0$.

The trapping potential is harmonic in all three directions, but strongly asymmetric concerning the radial (ρ) and axial (x) directions. In fact, the trapping frequencies are respectively $\nu_\rho = 2$ kHz and $\nu_x = 20$ Hz, yielding an elongated system (cigar-shaped) with inhomogeneous density. The spatial size of the system is given by the Thomas-Fermi radii $R_\rho = 2$ µm and $R_x = 200$ µm. This particular setup is helpful for suppressing the radial spin dynamics of the condensate and thus being able to study its longitudinal properties.

In order to extract the density distribution, the two spin states are treated independently one from another, and two imaging sequences are obtained at the end of each experimental realization. Then, an integration along the transverse direction is performed, obtaining two 1D density profiles $n_\uparrow(x)$ and $n_\downarrow(x)$, from which one can extract the relative magnetization

$$Z(x) = \frac{n_\uparrow(x) - n_\downarrow(x)}{n_\uparrow(x) + n_\downarrow(x)}\,. \tag{2.1}$$

It is possible to study the two-component system by separating the treatment on the density ($n = n_\uparrow + n_\downarrow$) and the spin ($nZ = n_\uparrow - n_\downarrow$) degrees of of freedom.

2.2 Data

Raw data is organized in a hierarchical system. At a fixed instant, the condensate's measured data are called a *shot* (it refers to the imaging process). Each shot is part of a series of them

that can be analyzed as the time evolution of a single system: this series is called a *sequence*. Eventually, during a *day* of measurements, many sequences may be collected, and a selection of them will be studied in the following analysis. For each sequence, the experimental data contains also the radiation coupling Ω_R in a range between 200 and 800 Hz (it changes from one day of measurements to another) and the detuning δ.

A shot contains all the information on the system at a certain instant, including the two population densities, $n_\uparrow(x)$ for to the atoms in the state $|\uparrow\rangle$ and $n_\downarrow(x)$ for the atoms in the state $|\downarrow\rangle$, distributed on a length scale from 0 to 400 pixels. The spatial resolution of the image is 1 pixel $= 1$ µm, so the two length units will be often used interchangeably. The magnetization data $Z(x)$ is calculated with Eq. (2.1) and, by definition, composed of a series of values ranging from -1 to 1.

Our focus here is to study the magnetization of the system, developing a method to analyze the effects of its bubble formation, and then proceed with the density behaviour.

2.2.1 Bubble parameters and shot sorting

In order to study the bubble dynamics, the most interesting parameters to retrieve from a shot are the bubble center x_0 and width σ_B. However, not all shots contain a bubble, namely the ones taken when the bubble was not formed yet. We can easily classify the two types of shots by computing the magnetization average in the central region and using a threshold value of $Z_{\text{thr}} = -0.2$. The no-bubble shots will be useful later, when dealing with the noise frequency spectrum.

To find the bubble parameters, the magnetization data is fitted with a double-arctangent function

$$Z_{\text{fit}}(x) = -A\left[\frac{2}{\pi}\arctan\left(\frac{x-c_1}{w_1}\right) - \frac{2}{\pi}\arctan\left(\frac{x-c_2}{w_2}\right)\right] + \Delta\,, \tag{2.2}$$

where c_1 and c_2 are the centers of the arctangent "shoulders", and w_1 and w_2 are their characteristic widths. Then, for a better result, a further fit is performed on each shoulder with a single-arctangent function

$$Z_{\text{fit}}(x) = -A\frac{2}{\pi}\arctan\left(\frac{x-c}{w}\right) + \Delta\,,$$

yielding the shoulder center c. Eventually, we obtain the bubble center $x_0 = (c_1 + c_2)/2$ and the bubble width $\sigma_B = c_2 - c_1$.

While this routine is very accurate for determining the shoulder profile and hence the bubble width, the transition between the shoulders and the inside region shows no continuity in many shots. In order to catch the entire profile and especially the boundaries of the inside region, we can fit the data with a piecewise function made of two exponential tails and a constant value in the middle, such as

$$Z_{\text{fit}}(x) = \begin{cases} A\exp\left(\frac{x-x_1}{w_1}\right) + \Delta & \text{for } x < x_1 \\ A + \Delta & \text{for } x_1 < x < x_2 \\ A\exp\left(-\frac{x-x_2}{w_2}\right) + \Delta & \text{for } x > x_2 \end{cases}$$

An example of fitting with the arctangent functions is provided in Fig. 2.1, while a gaussian fit is shown in Fig. 2.2.

Once the width is retrieved, it is useful to order the shots in a sequence by this parameter. This process lets us display the system evolution, in contrast to the original shot ordering based

Figure 2.1: Example of double arctangent fit results performed on a shot.

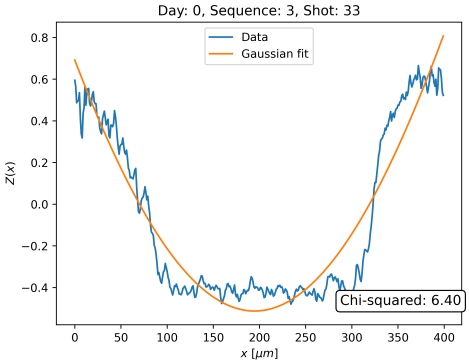

Figure 2.2: Example of gaussian fit results performed on a shot.

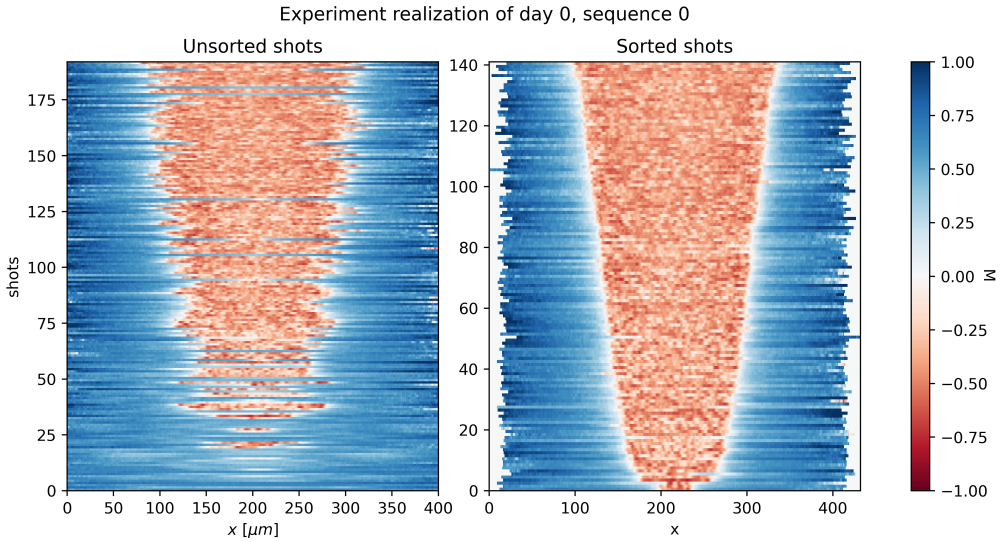

Figure 2.3: Shot sorting based on bubble width and alignment based on bubble center. Both parameters are estimated from the previous fitting procedure.

on the experimental time waited before observing the bubble. Furthermore, we can obtain a nicer picture by aligning the bubbles to their center and removing the no-bubble shots. An example sequence is shown in Fig. 2.3 with a colormap displaying the magnetization profiles (blue is for positive Z and red for negative Z).

2.2.2 FFT and ACF analysis

Since we are interested in the dynamics of the bubble, energy propagation is an important feature to focus on. In order to study it, a spectral profile is much needed, from which one can extrapolate the main frequencies of the signal.

We will first approach the problem of deriving such a profile using Fast Fourier Transform (FFT), an algorithm that implements the Discrete Fourier Transform (DFT) in an efficient manner. Given the input as a sequence of N discrete values $Z_0, \dots, Z_{N-1}$ sampled with spacing Δx, by definition the DFT is a series of N discrete values $\mathcal{Z}_0, \dots, \mathcal{Z}_{N-1}$ spaced by $\Delta k = 1/(N\Delta x)$ and convoluted with a complex phase such that

$$\mathcal{Z}_k = \sum_{n=0}^{n=N-1} Z_n e^{-2\pi i \frac{k}{N} n} .$$

When the input Z_n is real-valued, the transform is too, and it is also symmetric between positive and negative frequencies. The physical world contains only positive frequencies, so we will neglect the negative part of the transform.[1]

Another tool that can be used to study the periodic properties of a signal is the autocorrelation function (ACF). Similarly to the DFT, the ACF is also a particular type of convolution, where the signal is convoluted with itself. The caveat here is that since our signal is of finite length, the whole convolution would show boundary effects, as shown in Fig. 2.4. It is then

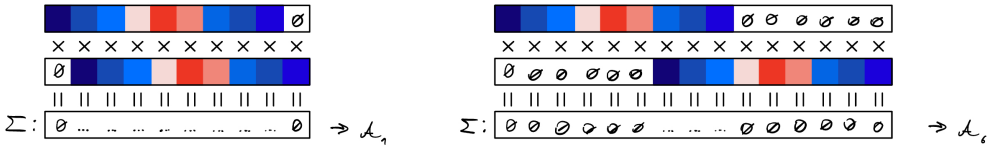

Figure 2.4: Boundary effects when computing the autocorrelation function on the whole signal. Since the signal is finite, the contributions on the borders are zero.

worth to limit the signal in a central window of length $2W$ and computing the ACF on the windowed signal. Taking as input the latter as $Z_0, \dots, Z_{2W-1}$, the output will be a series of values $\mathcal{A}_0, \dots, \mathcal{A}_W$ living in the spatial domain[2] such that:

$$\mathcal{A}_k = \frac{1}{2} \left(\frac{\sum_n Z_n Z_{n+k}}{\sqrt{\sum_n Z_n^2 \sum_n Z_{n+k}^2}} + \frac{\sum_n Z_n Z_{n-k}}{\sqrt{\sum_n Z_n^2 \sum_n Z_{n-k}^2}} \right) .$$

This formula computes the windowed autocorrelation by shifting the signal both to the left and to the right and then taking the average. Both terms are normalized in order to get $\mathcal{A}_0 = 1$.

Now, what we shall do is to compute the FFT and the ACF on the data, taking care of the fact that it is necessary to separate the inside region (the bubble) from the outside one and look for periodic signals in both. We will also compute the transforms on the no-bubble shots. An example of the inside region analysis is presented in Fig. 2.5. One can probably (with a good eye) already see in the colormap plot that two or three vertical bands extend over all shots and appear at the same frequencies. This ensures that the FFT averaging is rightful.

2.2.3 Border alignment

[1] This is achievable in `Python` using the function `rfft` instead of `fft`.

[2] While the FFT domain is made of frequencies, the ACF domain is instead made of lag values, corresponding to the spatial shifts of the signal.

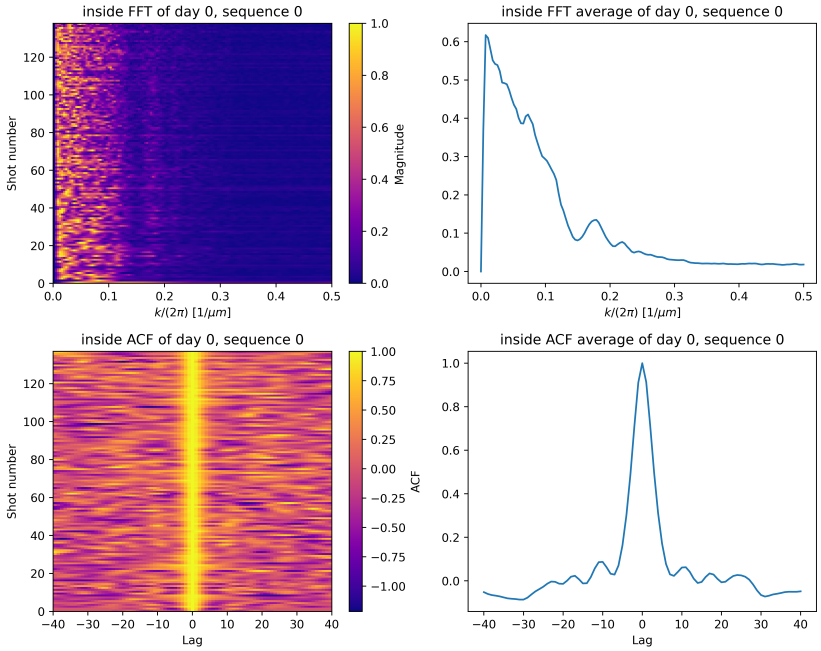

Figure 2.5: Example of FFT and ACF calculated in a sequence. The values for each shot are shown in the left plots with colormaps, while the averages are on the right.

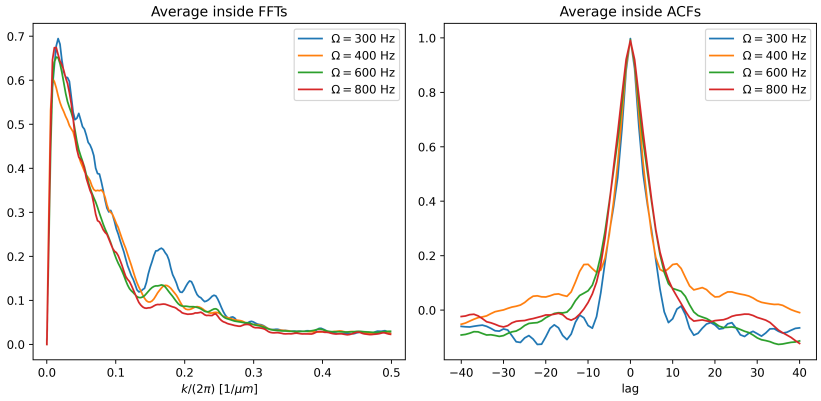

Figure 2.6: FFT and ACF profiles averaged over all sequences with the same radiation coupling Ω_R.

Conclusions

Bibliography

[1] Giacomo Lamporesi. "Two-component spin mixtures". In: *arXiv preprint arXiv:2304.03711* (2023).

[2] Lev Pitaevskii and Sandro Stringari. *Bose-Einstein condensation and superfluidity*. Vol. 164. Oxford University Press, 2016.

[3] Alessandro Zenesini et al. "False vacuum decay via bubble formation in ferromagnetic superfluids". In: *Nature Physics* (2024), pp. 1–6.

List of Figures

1.1 GPE simulation of a two-component balanced mixture in a harmonic potential. The shaded purple region shows the density distribution of population a and the yellow one the population b. Here, a small magnetic field is used to break the left-right simmetry. The total density profile is drawn in black. 7
1.2 Mean field energy and bubble formation. 8

2.1 Example of double arctangent fit results performed on a shot. 11
2.2 Example of gaussian fit results performed on a shot. 11
2.3 Shot sorting based on bubble width and alignment based on bubble center. Both parameters are estimated from the previous fitting procedure. 11
2.4 Boundary effects when computing the autocorrelation function on the whole signal. Since the signal is finite, the contributions on the borders are zero. 12
2.5 Example of FFT and ACF calculated in a sequence. The values for each shot are shown in the left plots with colormaps, while the averages are on the right. . . . 13
2.6 FFT and ACF profiles averaged over all sequences with the same radiation coupling Ω_R. 13